The nature of the variable millimetre–selected AGN in the brightest cluster galaxy of Abell 851

R. A. Cheale,[1]⋆ J. E. Geach,[1] A. C. Edge,[2] Y. C. Perrott[3] and T. Cantwell[4]

[1]*Center for Astrophysics Research, School of Physics, Astronomy & Mathematics, University of Hertfordshire, Hatfield, AL10 9AB, UK*
[2]*Centre for Extragalactic Astronomy, Department of Physics, Durham University, South Road, Durham, DH1 3LE, UK*
[3]*Astrophysics Group, Cavendish Laboratory, 19 J. J. Thomson Avenue, Cambridge CB3 0HE, UK*
[4]*Jodrell Bank Centre for Astrophysics, Alan Turing Building, School of Physics and Astronomy, University of Manchester, Manchester, M13 9PL, UK*

ABSTRACT

We present the detection of a bright 3 mm continuum source in the brightest cluster galaxy (BCG) in Abell 0851 ($z = 0.411$) with the NOrthern Extended Millimeter Array (NOEMA). When this detection is compared to other multifrequency observations across 21 cm–100 μm, including new Arcminute Microkelvin Imager 15 GHz observations, we find evidence for a relatively flat, variable core source associated with the BCG. The radio power and amplitude of variability observed in this galaxy is consistent with the cores in lower redshift BCGs in X-ray–selected clusters, and the flat mm–cm spectrum is suggestive of the BCG being a low-luminosity active galactic nucleus archetype. The discovery of this system could provide a basis for a long-term study of the role of low-luminosity radio mode 'regulatory' feedback in massive clusters.

Key words: techniques: interferometric – galaxies: clusters: individual: (A851, Cl 0939+4713) – galaxies: clusters: individual: Abell 851 – galaxies: elliptical and lenticular, cD – galaxies: evolution.

1 INTRODUCTION

The discovery that every massive galaxy contains a supermassive black hole (SMBH), and that the masses of the stellar bulge and SMBH are correlated (Magorrian et al. 1998; Silk & Rees 1998) demonstrates that the growth of the central black hole and its host galaxy are inexorably linked. Black hole accretion releases large amounts of feedback energy and momentum into the interstellar medium (and beyond) via collimated jets and fast winds driven from the hot accretion disc, and is thought to be a driving feature in the regulation of stellar mass growth (Bower et al. 2006; Croton et al. 2006). Active Galactic Nucleus (AGN) feedback is now an established feature of galaxy formation models that are required to correctly reproduce the key observable features of the local galaxy population (e.g. Sijacki et al. 2007; Booth & Schaye 2009; Fabian 2012; Ishibashi & Fabian 2012)

We observe a wide range of nuclear activity in galaxies; from low luminosity or quiescent systems such as Sgr A⋆ at the centre of the Milky Way, up to powerful radio galaxies and quasars where AGN feedback can expel large fractions of the gas reservoir and pump energy into the circumgalactic and intergalactic medium (Gaspari et al. 2011; Dubois et al. 2013; Schaye et al. 2015). This substantial energy input into the local environment is necessary for regulat-

ing stellar mass growth on galaxy scales by stifling the cooling of intracluster gas(see; Fabian 2012), but this must be sustained for many Gyr to maintain the suppression of stellar mass growth in the host galaxy (Dunn & Fabian 2008). It is likely that a self-regulating process affects the growth of the central black hole, as exhibited in numerical simulations (e.g. Springel, Di Matteo & Hernquist 2005) and galaxy formation theories (Silk & Rees 1998; Benson 2010).

Variability is associated with all AGN from high-luminosity quasars to Seyfert galaxies (McHardy et al. 2006). Low-luminosity AGN (LLAGN), like Sgr A⋆, M81 (Sakamoto et al. 2001; Schodel et al. 2007), Centaurus A (Israel et al. 2008), and NGC 7469 (Baldi et al. 2015) have relatively low-Eddington rates ($L \approx 0.1 \, L_{\rm Edd}$) and often exhibit bright inverted/flat cm–mm spectra likely originating from a compact core (e.g. Behar et al. 2018). Recent advances in mm-interferometry in resolution and sensitivity make the detection of such LLAGN more probable. Indeed, work by Doi et al. 2011 supports the view that many large passive galaxies have compact millimetre cores with significant variable radio activity at their cores, but few systematic searches for such LLAGN have yet been made, and in general the detection and monitoring of AGN variability requires multiple observations over weeks to decades.

Here we present evidence of a variable AGN in the well-known cluster Abell 851 (also known as CL 0939+4713), a rich (Seitz et al. 1996) cluster ($M \sim 10^{14} \, {\rm M_\odot}$ at $z = 0.411$ containing several hundred spectroscopically classified members (Dressler & Gunn
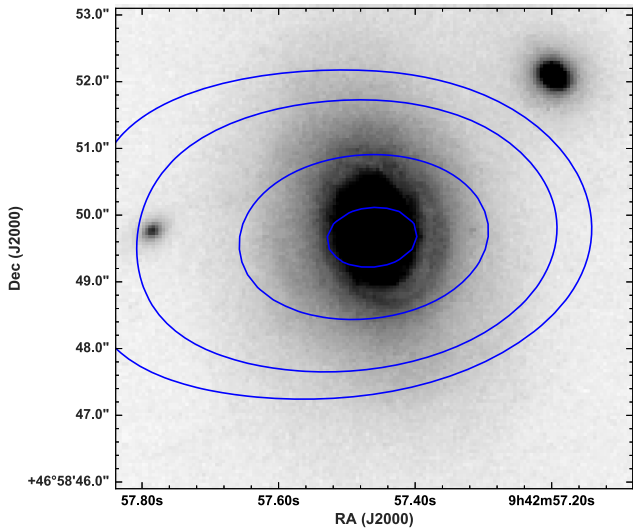
⋆ E-mail: ryan.ac@live.com

Figure 1. The archival *HST*/ACS F814W filter optical imaging. DG92-311 is located α; $09^h\,42^m\,57.50^s$, δ; $46^d\,48^m\,50.00^s$. The primary beam corrected significance contours are overlayed, initiating at 1.05 mJy (3σ) and increasing in 1σ intervals. We find a corrected (see Section 2.2) peak flux density of $S_{3.6mm}$ 1.59 ± 0.15 mJy.

1992). The galaxy in question is a possible Sa/S0 transition object close to the cluster centre, catalogued by Dressler & Gunn (1992) as object 311 and hence referred to in this paper as DG92-311. DG92-311 is optically classified as an early-type disc (Sa/S0) with post-starburst spectral features; namely weak nebular emission but relatively strong Balmer absorption ((k+a) Belloni et al. 1995; Dressler et al. 1999; Oemler et al. 2009). In this letter, we present the observational evidence across the radio-far-infrared spectral energy distribution of DG92-311, including new 3 mm IRAM Plateau de Bure interferometer and new 1.9 cm Arcminute Microkelvin Imager observations. Throughout we assume a ΛCDM cosmology with $H_0 = 67.3$ km s^{-1} Mpc^{-1}, $\Omega_M = 0.315$, and $\Omega_\Lambda = 0.685$ (Planck Collaboration et al. 2016).

2 DATA COLLECTION AND ANALYSIS

We use a number of archival observations of DG92-311 including *WISE* 3.4–22 μm, *Herschel* PACS and SPIRE 100–500μm, James Clerk Maxwell Telescope (JCMT) SCUBA 850μm (project M00BH05), BIMA 1.05 cm, AMI 1.9 cm, and VLA/FIRST 6.2–21 cm band archives. The *HST*/ACS F814W filter optical imaging is shown in Fig. 1 (data retrieved from the MAST archive *HST*, project 10418). We report the various flux density measurements of DG92-311 in Table 1.

2.1 Archival data

2.1.1 JCMT/SCUBA

Observations of DG92-311 by SCUBA at 850 μm were conducted on 2000 November 27. The target was observed in the 'jiggle' map mode used for observing sources smaller than the array (Jenness et al. 2000). The target is formally undetected in the archival map, and so we determine an upper limit by sampling a large number of random pixels around the source position and fit a Gaussian to the resulting pixel distribution. We take the standard deviation of the

Gaussian as a measure the 1σ noise, and determine a 3σ upper limit of $S_{850\mu m} < 4.6$ mJy for DG92-311.

2.1.2 Herschel Lensing Survey

The *Herschel* Lensing Survey (HLS Egami et al. 2010) observed Abell 851 with the PACS (100 and 160 μm) and SPIRE (250, 350, and 500 μm) instruments. These far-IR/sub-mm bands are useful to constrain the peak of the thermal dust emission. Rawle et al. (2012) analyse a number of BCGs from the HLS including A851. Photometry in the SPIRE bands was reduced by using the IRAF package ALLSTAR (Tody 1993) by fitting the Point Spread Function to source locations. In the PACS, bands fluxes were measured by using aperture photometry with the use of SEXTRACTOR (Bertin & Arnouts 1996); methods are described in detail in Rawle et al. DG92-311 was detected in all but the 500 μm band, and we report the measurements in Table 1.

2.2 NOEMA observations

In project S14BV (PI: Geach), we observed DG92-311 as part of a larger 3 mm mosaic of Abell 851 to search for co(2–1) emission associated with cluster members (e.g. Geach et al. 2009). Abell 851 was observed in configuration D (baseline separations up to 150 m) for maximum sensitivity. We adopted a similar set up to Geach et al. (2009), where the 3 mm receiver was set to the frequency of the redshifted CO(1-0) line at the redshift of the cluster, and the correlator was set up with 2.5-MHz spacing (2 × 64 channels, 320-MHz bandwidth). The data were reduced using the standard Grenoble Image and Line Data Analysis Software (GILDAS[1]) and converted to a UVFITS data table for imaging in the CASA environment (McMullin et al. 2007). The 3 mm continuum detection became obvious in a channel-by-channel inspection of the data cube. We note the source lies close to the edge of the 50 arcsec primary beam, and we apply an appropriate primary beam correction to measure a flux density $S_{3.6\,mm} = 2.6 \pm 0.4$ mJy. The 3 mm contours are overlaid on *HST*/ACS optical imaging in Fig. 1.

2.3 The Arcminute Microkelvin Imager

The Arcminute Microkelvin Imager (AMI; Zwart et al. 2008; Hickish et al. 2018) is a dual aperture-synthesis array that operates between 13.9–18.2 GHz with 2048 channels. The principle use of the AMI detector is for imaging the Sunyaev–Zel'dovich effect by observing galaxy clusters. However, we make use of the instrument for its favourable bandwidth for observations pointed at A851. DG92-311 was observed by AMI on 2017 October 4 with an integration time of 7200 s, we make use of AMI-LA with angular resolution of 30 arcsec using seven of the eight 12.8 m diameter dishes.

The AMI-LA data were calibrated and imaged in CASA. Primary calibration was performed using a nearby observation of 3C 286, using the (Perley & Butler 2013a) flux density scale along with a correction for the fact that AMI measures I+Q, using the polarization fraction and angle fits from Perley & Butler (2013b); this is an ≈ 4.5 per cent correction for 3C 286 over the AMI band. The primary calibration observation supplied an instrumental bandpass in both phase and amplitude. This was applied to the target data, as well as a correction for atmospheric amplitude variations produced by the 'rain gauge', which is a noise injection system used to

[1]http://www.iram.fr/IRAMFR/GILDAS

Table 1. Observed bands for Abell 851, the flux density (S), and uncertainty (δS) for each wavelength is provided in column 3 and 4.

Instrument	Angular Resolution	Wavelength	S (mJy)	δS (mJy)	Reference	Observation Date
WISE	6.1 arcsec	3.4 μm	0.48	0.02	Wright et al. 2010	2010–2013
WISE	6.4 arcsec	4.6 μm	0.31	0.02	Wright et al. 2010	2010–2013
WISE	6.5 arcsec	12 μm	0.60	0.17	Wright et al. 2010	2010–2013
WISE	12 arcsec	22 μm	<3.0	—	Wright et al. 2010	2010–2013
PACS	8 arcsec	100 μm	23.7	0.3	Rawle et al. 2012	2003-07-01
PACS	13 arcsec	160 μm	25.3	0.7	Rawle et al. 2012	2003-07-01
SPIRE	18 arcsec	250 μm	20.5	5.5	Rawle et al. 2012	2003-07-01
SPIRE	25 arcsec	350 μm	12.3	6.2	Rawle et al. 2012	2003-07-01
SPIRE	36 arcsec	500 μm	<11.0	—	Rawle et al. 2012	2003-07-01
SCUBA	14 arcsec	850 μm	<4.6	—	Smail et al. 2002	2000-11-27
IRAM PdBI	6 arcsec	3.6 mm	2.59	0.40	This work	2014-06-07
BIMA	23 arcsec	1.05 cm	1.06	0.15	Coble et al. 2007	1997-07-15
AMI-LA	30 arcsec	1.9 cm	2.2	0.1	Hurley-Walker et al. 2012	2008-2009
AMI-LA	30 arcsec	1.9 cm	3.46	0.09	This work	2017-10-04
VLA	4 arcsec	6.2 cm	3.01	0.14	Archive3	1990-12-01
VLA	4 arcsec	6.2 cm	2.79	0.03	Archive3	1993-08-28
VLA	4 arcsec	21 cm	1.6	0.16	Morrison 1999	1996-01-06
VLA/FIRST	4 arcsec	21 cm	2.13	0.31	White et al. 1997	1997-03-25
VLA	4 arcsec	21 cm	3.1	0.2	Condon, Dickey & Salpeter 1990	1987-05-23

measure the atmospheric noise contribution (see Zwart et al. 2008). The nearby bright point source 5C 5.175 was observed throughout the observation in an interleaved manner and was used to correct for atmospheric and/or instrumental phase drift. After narrow-band RFI flagging, the data were binned down to 64 channels to reduce processing time and imaged at the central frequency, 15.5 GHz. We used the 'clean' task, using multifrequency synthesis with nterms = 2 which allows for a frequency dependence of the sky brightness. We used the CASA graphical Gaussian fitting task on the resulting image to confirm that the source was unresolved and measure a peak flux density of signal of $S_{1.9\ \mathrm{cm}} = 3.46 \pm 0.09$ mJy including thermal noise and a 5 per cent systematic error estimate at 15.5 GHz (1.9 cm). Hurley-Walker et al. (2012, HW12) also observed cluster A851 in 2012 with AMI-LA reporting $S_{\mathrm{LA}} = 2.2 \pm 0.1$ at the position of DG92-311 (table 12, ID B in HW12) we include both results in Table 1.

3 ANALYSIS AND DISCUSSION

3.1 Spectral energy distribution

In Fig. 2, we construct the spectral energy distribution using the data in Table 1 and fit three components spanning the radio, sub-mm, and far-IR bands. Note that, despite the data spanning a range of angular resolutions, all observations are unresolved for DG92-311 and a comparison of the beam sizes to the optical imaging of DG92-311 shows that we are in all cases measuring galaxy-integrated flux densities with negligible contamination from neighbouring or background sources.

The *Herschel* 100–350 μm flux measurements allow for a simple least squares fit of an isothermal modified blackbody, where we employ a standard emissivity term, $\beta = 1.5$ (Hildebrand 1983; Casey 2012), allowing dust temperature as the free parameter. We find a best-fitting dust temperature of $T_D = 24$ K, consistent with the S0 morphological–temperature results found by Bendo et al. (2003). We also make use of the well-known FIR/sub-mm templates described by Dale & Helou (2002) to fit the 100–350 μm data. We
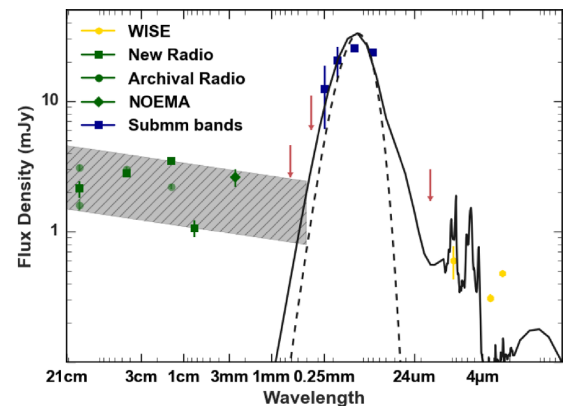

Figure 2. The rest-frame spectral energy distribution for DG92-311. The blue squares cover the sub-mm wavebands: 100, 160, 250, 350, 500, and 850 μm, the green diamond is the imaged IRAM PdBI 3.6 mm detection, the gold hexagons are the FIR WISE bands, green squares are the most recent radio observations whereas the fainter green circles are historic observations (listed in Table 1). The shaded region shows the synchrotron emission amplitude range of a source with $\alpha \approx -0.1$ over two decades, the black dashed line is thermal blackbody component fit with a characteristic temperature of $T = 24$ K and, finally, the black solid line is a SPIRE 250 μm normalized template with $\alpha = 3.125$ from Dale & Helou 2002.

normalize to the 160 μm PACS detection as it lies near the peak of the thermal emission and we overlay the template which is best suited to the *Herschel* data (corresponding to a power-law index of $\alpha = 1.875$), as a solid black curve.

In the radio bands, the spectral index of the synchrotron power-law component is estimated from the ratio of the most recent NOEMA 3 mm and the average AMI 1.9 cm observations, giving $\alpha \approx -0.1$ for $S \propto \nu^{\alpha}$. We overlay a grey hashed region on to Fig. 2 to represent the range of flux normalizations that fit the full range of radio observations up to the Rayleigh–Jeans tail of the thermal dust emission. While it is very likely that the synchrotron component will have some spectral curvature over the three orders of magnitude in
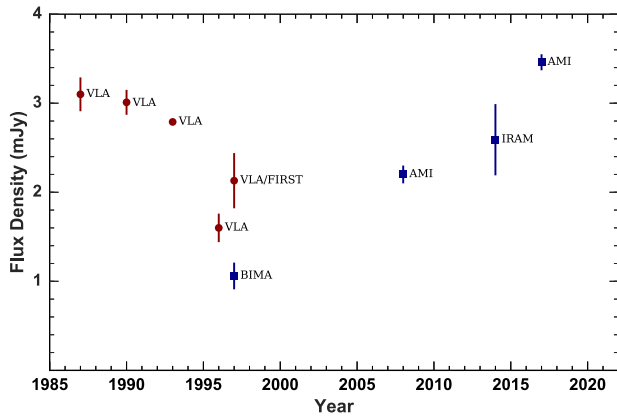
Figure 3. Two decades of radio data from VLA, BIMA, AMI, and IRAM reveals an up-turn in the BCG light curve. We derive out spectral index from the most recent observations by AMI and IRAM-PdBI. Red squares indicate data ≥ 10 GHz and blue circles < 10 GHz. It is clear from the figure that at < 10 GHz there has been a gradual decline in luminosity but in bands ≥ 10 GHz there is evidence of an increase.

frequency plotted (Hogan et al. 2015b), as we lack simultaneous observations over the full spectral range then we must interpret any variability assuming a single power-law index, as we discuss in the next section.

3.2 Variability

The radio light curves with observations from VLA, BIMA, AMI, and NOEMA spanning near two decades in time is shown in Fig. 3. The source exhibits a flat spectrum over 1.4–82 GHz range and is unlikely to be extended on the >few arcsecond scales of the resolution of the majority of observations (Table 1). Although none of these data were taken simultaneously, it is clear that over the 1.4–82 GHz frequency range covered there has been a significant change in the normalization of the power-law synchrotron component over the past 20–30 yr. The source varies at the same frequency and resolution in data from both the VLA at 1.4 GHz and AMI-LA at 15 GHz; furthermore, the NOEMA data has better angular resolution than the BIMA and AMI-LA data but is brighter than all but the most recent AMI-LA point. If flux were being missed on larger scales, then one would expect the 3 mm point to be fainter. The source appears to have been at a minimum around the year 2000 and has gradually increased in brightness by a factor of more than three in the past 18 yr. We argue that the observed radio variability is intrinsic to the source.

This magnitude and time-scale for radio variability is observed in local BCGs such as NGC 1275 in the Perseus cluster (Dutson et al. 2014) and a sample of bright, flat spectrum cores monitored with the OVRO 40m (Hogan et al. 2015b). All of these variable BCGs are found in dusty BCGs with luminous optical lines in cool core clusters (Hogan et al. 2015b) with no evidence for jet contribution. As can be seen from the *HST* optical imaging in Fig. 1, DG92-311 does exhibit dust lanes and the bright sub-mm detections across the *Herschel* bands indicate the presence of dust in the interstellar medium. DG92-311 does not exhibit any significant Hα line emission (Koyama et al. 2011) and, although there is no *Chandra* observation of A851 and DG92-311 falls on a chip-gap of the EPIC camera in the only onaxis pointing with *XMM–Newton*, the wider structure of the cluster in the X-ray from *ROSAT* (Schindler et al. 1998) suggests that any cool core in A851 is weak. On this basis

DG92-311 is atypical of BCGs with a strong radio core. The observed radio power of DG92-311 of $\approx 10^{24}$ W Hz^{-1} implies that it falls in the upper quartile of core radio power of all X-ray luminous clusters (Hogan et al. 2015a) with a cool core or in the uppermost 3 per cent of core radio power for BCGs without a surrounding cool core. While the observed radio variability could be due to a jet, the similarity in its amplitude and time-scale implies a similar origin for the core emission in other BCGs. Therefore DG92-311 is an important system that may have an unusual X-ray environment, and therefore more detailed X-ray follow-up is required to determine the properties of the intracluster gas on scales of 10s kpc around the BCG.

4 CONCLUSIONS

Optically, DG92-311 appears to be a relatively unremarkable, dusty early-type disc galaxy (Sa/S0) but when observed in the radio–submillimetre this optically inactive galaxy appears to contain a relatively powerful, variable LLAGN in what is the Brightest Cluster Galaxy in a rich cluster. While the variability of a factor of three on decade time-scales is consistent with other BCGs, the lack of a prominent cool core in the host cluster is surprising and highlights the need to assess the temporal behaviour of all massive galaxies in cluster cores, particularly in the millimetre wavelengths, to ascertain the underlying level radio mode regulatory feedback in massive clusters.

REFERENCES

Baldi R. D., Behar E., Laor A., Horesh A., 2015, MNRAS, 454, 4277
Behar E., Vogel S., Baldi R. D., Smith K. L., Mushotzky R. F., 2018, MNRAS, 478, 399
Belloni P., Bruzual A. G., Thimm G. J., Roser H.-J., 1995, A&A, 297, 61
Bendo G. J. et al., 2003, AJ, 125, 2361
Benson A. J., 2010, Phys. Rep., 495, 33
Bertin E., Arnouts S., 1996, A&AS, 117, 393
Booth C. M., Schaye J., 2009, MNRAS, 398, 53
Bower R. G., Benson A. J., Malbon R., Helly J. C., Frenk C. S., Baugh C. M., Cole S., Lacey C. G., 2006, MNRAS, 370, 645
Casey C. M., 2012, MNRAS, 425, 3094
Coble K. et al., 2007, AJ, 134, 897
Condon J. J., Dickey J. M., Salpeter E. E., 1990, AJ, 99, 1071
Croton D. J. et al., 2006, MNRAS, 365, 11
Dale D. A., Helou G., 2002, ApJ, 576, 159

Doi A., Nakanishi K., Nagai H., Kohno K., Kameno S., 2011, AJ, 142, 167

Dressler A., Gunn J. E., 1992, ApJS, 78, 1

Dressler A., Smail I., Poggianti B., Butcher H., Couch W., Ellis R., Oemler A., Jr, 1999, ApJS, 122, 51

Dubois Y., Pichon C., Devriendt J., Silk J., Haehnelt M., Kimm T., Slyz A., 2013, MNRAS, 428, 2885

Dunn R. J. H., Fabian A. C., 2008, MNRAS, 385, 757

Dutson K. L., Edge A. C., Hinton J. A., Hogan M. T., Gurwell M. A., Alston W. N., 2014, MNRAS, 442, 2048

Egami E. et al., 2010, A&A, 518, L12

Fabian A. C., 2012, ARA&A, 50, 455

Gaspari M., Brighenti F., D'Ercole A., Melioli C., 2011, MNRAS, 415, 1549

Geach J. E. et al., 2009, MNRAS, 395:62

Hickish J. et al., 2018, MNRAS, 475, 5677

Hildebrand R. H., 1983, QJRAS, 24, 267

Hogan M. T. et al., 2015a, MNRAS, 453, 1201

Hogan M. T. et al., 2015b, MNRAS, 453, 1223

Hurley-Walker N. et al., 2012, MNRAS, 419, 2921

Ishibashi W., Fabian A. C., 2012, MNRAS, 427, 2998

Israel F. P., Raban D., Booth R. S., Rantakyr F. T., 2008, A&A, 483, 741

Jenness T., Lightfoot J. F., Holland W. S., Greaves J. S., Economou F., 2000, in Mangum J. G., Radford S. J. E., eds, ASP Conf. Ser. Vol. 217, Imaging at Radio through Submillimeter Wavelengths. Astron. Soc. Pac., San Francisco, p. 205

Koyama Y., Kodama T., Nakata F., Shimasaku K., Okamura S., 2011, ApJ, 734, 66

Magorrian J. et al., 1998, AJ, 115, 2285

McHardy I. M., Koerding E., Knigge C., Uttley P., Fender R. P., 2006, Nature, 444, 730

McMullin J. P., Waters B., Schiebel D., Young W., Golap K., 2007, in Shaw R. A., ed., ASP Conf. Ser. Vol. 376, Astronomical Data Analysis Software and Systems XVI. Astron. Soc. Pac., San Francisco, p. 127

Morrison G. E., 1999, Ph.D. Thesis

Oemler A., Jr, Dressler A., Kelson D., Rigby J., Poggianti B. M., Fritz J., Morrison G., Smail I., 2009, ApJ, 696, 1063

Perley R. A., Butler B. J., 2013a, ApJS, 204, 19

Perley R. A., Butler B. J., 2013b, ApJS, 206, 16

Planck Collaboration et al., 2016, A&A, 594, A1

Rawle T. D. et al., 2012, ApJ, 747, 29

Sakamoto K., Fukuda H., Wada K., Habe A., 2001, AJ, 122, 1319

Schaye J. et al., 2015, MNRAS, 446, 521

Schindler S., Belloni P., Ikebe Y., Hattori M., Wambsganss J., Tanaka Y., 1998, A&A, 338, 843

Schodel R., Krips M., Markoff S., Neri R., Eckart A., 2007, A&A, 463, 551

Seitz C., Kneib J.-P., Schneider P., Seitz S., 1996, A&A, 314, L707

Sijacki D., Springel V., Di Matteo T., Hernquist L., 2007, MNRAS, 380, 877

Silk J., Rees M. J., 1998, A&A, 331, L1

Smail I., Ivison R. J., Blain A. W., Kneib J.-P., 2002, MNRAS, 331, 495

Springel V., Di Matteo T., Hernquist L., 2005, MNRAS, 361, 776

Tody D., 1993, in Hanisch R. J., Brissenden R. J. V., Barnes J., eds, ASP Conf. Ser. Vol. 52, IRAF in the Nineties. Astron. Soc. Pac., San Francisco, p. 173

White R. L., Becker R. H., Helfand D. J., Gregg M. D., 1997, ApJ, 475, 479

Wright E. L. et al., 2010, AJ, 140, 1868

Zwart J. T. L. et al., 2008, MNRAS, 391, 1545

This paper has been typeset from a T_EX/L^AT_EX file prepared by the author.